Steel and Composite Structures, *Vol. 48, No. 4 (2023) 461-474*
https://doi.org/10.12989/scs.2023.48.4.461

Ultimate compressive strength predictions of CFT considering the nonlinear Poisson effect

Yu-A Kim[1], Ju-young Hwang[2] and Jin-Kook Kim*[1]

[1]Department of Civil Engineering, Seoul National University of Science and Technology, 232 Gongneung-ro, Nowon-gu, Seoul 01811, Republic of Korea
[2]Department of Civil Engineering, Dong-Eui University, Busan 47340, Republic of Korea

(Received November 1, 2022, Revised May 19, 2023, Accepted August 3, 2023)

Abstract. Concrete-filled steel tubes are among the most efficient compressive structural members because the strength of the concrete is enhanced given that the surrounding steel tube confines the concrete laterally and the steel tube is restrained with regard to inward deformation due to the concrete existing inside. Accurate estimations of the ultimate compressive strength of CFT are important for efficient designs of CFT members. In this study, an analytical procedure that directly formulates the interaction between the concrete and steel tube by considering the nonlinear Poisson effect and stress-strain curve of the concrete including the confinement effect is proposed. The failure stress of concrete and von-Mises failure yield criterion of steel were used to consider multi-dimensional stresses. To verify the prediction capabilities of the proposed analytical procedure, 99 circular CFT experimental data instances from other studies were used for a comparison with AISC, Eurocode 4, and other researchers' predictions. From the comparison, it was revealed that the proposed procedure more accurately predicted the ultimate compressive strength of a circular CFT regardless of the range of the design variables, in this case the concrete compressive strength, yield strength of the steel tube and diameter relative to the thickness ratio of the tube.

Keywords: CFT; confinement; hoop stress; nonlinear Poisson effect; ultimate strength

1. Introduction

Concrete-filled steel tubes (CFT) are a special structural element in that each material compensates for the weaknesses of other elements. Microcracks in concrete that occur under compression are laterally restrained by the steel tube, and this leads to higher stiffness and strength. The steel tube is restrained with regard to inward deformation due to the concrete, which delays local buckling in the tube. However, considering that the Poisson's ratio of concrete is smaller than that of steel in the linear elastic stress range, interaction between concrete and the tube cannot be expected under a service load condition. That is, there is no confinement of the concrete in low-stress level (Schneider 1998). Once microcracks occur at some compressive stress level, the stress-strain curve starts to show nonlinear behavior. Therefore, when concrete subjected to compressive loading is laterally confined or compressed, the occurrence of microcracks and growth will be delayed, thus extending the linear range of the stress-strain curve and enhancing the ultimate strength. This phenomenon is known as the confinement effect of concrete. In a CFT, when the Poisson's ratio of concrete exceeds that of the steel, interaction between the concrete and steel tube can be observed, and hoop stress in the reaction to the lateral expansion of concrete will confine the concrete.

*Corresponding author, Ph.D. Professor
E-mail: jinkook.kim@seoultech.ac.kr

Numerous studies have been conducted on the ultimate strength of concrete considering the confinement effect. In addition, CFT assessments considering the confinement effect based on experimental and numerical analyses have been done and formulas to predict the strength have been proposed (Knowles and Park 1969, Tang *et al.* 1997, Chen *et al.* 2018, Wang *et al.* 2019, Hasan *et al.* 2019, Wei *et al.* 2020, Fan *et al.* 2021, Luat *et al.* 2021).

Knowles and Park (1969) studied the ultimate strength of a slender CFT column subjected to axial and eccentric loads for a wide range of slenderness ratios. In their study, the confinement effect on the concrete was not found in the slender columns because buckling occurred before the concrete reached the level of inelastic high strain that would cause its volume to increase. That is, in their slender columns, the effect of the concrete compressive strength is negligible and, consequently, the confinement effect is not influential. Tang *et al.* (1997) included a Poisson's ratios correlation between the concrete and steel tube in their quantification of the confining pressure acting on the concrete. Based on experiments with the variables of the concrete compressive strength, steel tube yield strength, and D/t of the steel tube, the stress-strain relationship of concrete considering confinement was proposed.

Recently, Chen *et al.* (2018) conducted an axial load test of CFT reinforced with silica fume and steel fiber. They found that silica fume and steel fiber did not influence the mode of failure but did increase the ultimate compressive strength due to the additional confinement by the steel fiber and the pozzolanic action of the silica fume. Wang *et al.* (2019) conducted axial load tests of 20 CFT specimens in

http://www.techno-press.com/journals/scs&subpage=8
ISSN: 1229-9367 (Print), 1598-6233 (Online)

which the effects of the load conditions, the diameter-thickness ratio and the compressive strength of reactive powder concrete (RPC) were considered. In their results, they found that lateral confinement was provided only when the strain exceeded the yield limit. Hasan *et al.* (2019) performed axial load tests on 22 CFT specimens to observe the failure modes of CFT considering the influence of D/t ratio and number of steel rebars. The results show that the strengh of CFT increases with increasing number of steel reinforcing bars and the local buckling of columns decreases when the thickness of steel tube increases. Wei *et al.* (2020) used 107 experimental data instances for an analysis of the behavior of high-strength CFTs, among which 87 tests were from other studies and 20 tests were from an additional test in their to fill the gaps in the existing dataset. Using the data, they evaluated the design formulas of the ultimate compressive strength of CFTs. Fan *et al.* (2021) quantitatively investigated the compatibility of design variables such as the material strength (f_{ck}, f_y), diameter, and thickness of the tube in predictions of the ultimate axial strength. The concluded that small *D*/*t* and low f_y-high f_{ck} values should be avoided due to the low strength enhancement and provided the optimal combination of design variables. Luat *et al.* (2021) proposed a hybrid intelligence model, termed G-MARS, that incorporated a genetic algorithm and multivariate adaptive regression splines for predictions of the ultimate axial strength of CFTs. In their study, 504 experimental data instances were used for training and verification.

Despite the many previous studies as outlined above, most of them focused on the determination of the ultimate compressive strength based the results without considering detailed interactions between the materials involved. In addition, the previously proposed strength estimation equations of CFT can not quantitatively consider the confinement effect of steel tube because they do not consider the difference in the confinement force of steel tube according to the stress level due to the nonlinear Poisson ratio effect of concrete. However, in order to extend the use of efficient CFTs to various structural applications, understanding these detailed interactions is required, and an analytical procedure must be established to trace the interactive behavior of CFTs while they are gradually subjected to ultimate axial loading levels. In this study, an analytical procedure that directly formulates the interaction between the concrete and the steel tube by considering the nonlinear Poisson effect and the nonlinear stress-strain curve of the concrete, including the confinement effect, is proposed. Here, only short and compact cross-sections were considered to ignore the effects of local buckling and quantitatively estimate the effect of improving the strength of concrete due to the confinement force of steel tube. The failure stress from a biaxial interaction diagram of concrete and the von-Mises failure yield criterion were used to consider the multi-dimensional stresses acting on the concrete and steel tube, respectively. In order to verify the prediction capabilities of the proposed analytical procedure, 99 circular CFT experimental data instances from other studies were used for a comparison with AISC (2016), Eurocode 4 (2004), and prediction methods devised by other researchers.

Table 1 Design criteria for the width-to-thickness ratio for the steel tube of a CFT

	Circular steel tube		
	λ_p (compact/ Noncompact)	λ_r (Noncompact/Slender)	λ_{max} (Maximum permit)
AISC (2016)	$\frac{0.15E}{f_y}$	$\frac{0.19E}{f_y}$	$\frac{0.31E}{f_y}$
EC4 (2004)			$90\frac{235}{f_y}$
ACI (2019)			$\sqrt{\frac{8E}{f_y}}$

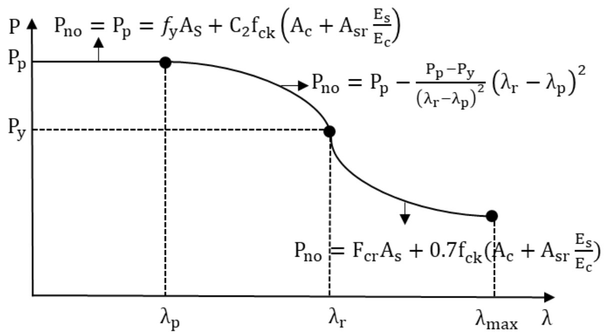

Fig. 1 Compressive strength according to the section type

2. Prediction formulas for the ultimate compressive strength of CFTs

2.1 AISC

AISC (2016) applies a different criteria for the width-to-thickness ratio according to the section shape of the CFT. AISC (2016) has three width-to-thickness ratio categories: (1) compact, (2) non-compact, and (3) slender, as shown in Table 1 and Fig. 1. The different *D*/*t* criteria of each design formula exist because each design formula uses a different method to consider the strength reduction for local buckling in the steel tube. AISC (2016) defines two strength formulas for compact and slender sections and applies interpolation for non-compact sections, as shown in Fig. 1. The compressive axial strength (P_p) of the CFT by AISC (2016) is determined by Eq. (1). In the formula, the confinement effect is considered to be constant regardless of *D*/*t* or f_y because the coefficient of f_{ck} is a constant, 0.95 for a compact section. Therefore, this formula may underestimate the ultimate axial strength of CFTs for sections that are highly influenced by the confinement effect.

$$P_p = f_y A_S + C_2 f_{ck}\left(A_c + A_{sr}\frac{E_s}{E_c}\right) \quad (1)$$

Here, f_y is the yield strength of the steel tube, A_S is the cross-sectional area of the steel tube, f_{ck} is the compressive strength of the concrete, A_c is the net area of

Table 2 Prediction formulas for the ultimate compressive strength of CFT by various researchers

Reference	Formulas
Sun (2008)	$N_u = f_{cc}A_c$, where $f_{cc} = f_{ck}(1 + 8.2\frac{(D/t-1)}{(D/t-2)^2}\frac{f_y}{f_{ck}})$
Liu *et al.* (2016)	$N_u = \sigma_v A_s + \sigma_{cp} A_c$ where $\sigma_v = 0.61 f_y$; $f_{cc} = f_{ck} + 4.1\sigma_r$; $\sigma_r = \frac{2t\sigma_h}{D-2t} = \frac{1.08 t f_y}{D}$; $\sigma_h = 0.54 f_y$
O'Shea and Bridge (2000)	$N_u = f_y A_s + \sigma_{cp} A_c$, where $D/t \le 200$ for $f_{ck} \le 50\ MPa$, $f_{cc} = f_{ck}\left(-1.228 + 2.172\sqrt{\frac{1+7.46 f_l}{f_{ck}}} - 2\frac{f_l}{f_{ck}}\right)$ for $80\ MPa \le f_{ck} \le 100\ MPa$, $\frac{f_{cc}}{f_{ck}} = \left(\frac{f_l}{f_t} + 1\right)^k$ $k = 1.25\left[1 + 0.062\frac{f_l}{f_{ck}}\right](f_{ck})^{-0.21}$; $f_t = 0.558\sqrt{f_{ck}}$

the concrete, A_{sr} is the area of the rebar, E_s is the modulus of elasticity of the steel, E_c is the modulus of elasticity of the concrete, and C_2 is the confinement coefficient (0.95) for a round section.

2.2 Eurocode 4

The compressive axial strength ($N_{pl,Rd}$) of a CFT by EC4 (2004) is determined by Eq. (2). In the formula, the concrete strength magnification coefficient is given as a function of the influential factors of D, t, f_{ck}, and f_y, and the coefficient is larger than 1.0. That is, once the criteria of the width-to-thickness ratio are met, the concrete is regarded as fully confined to develop at least the full compressive strength f_{ck}. In contrast to AISC (2016), EC4 (2004) can effectively consider both the confinement effect on the concrete and the strength reduction by local buckling.

$$N_{pl,Rd} = \eta_a A_s f_y + A_c f_{ck}\left(1 + \eta_c \frac{t}{D}\frac{f_y}{f_{ck}}\right) + A_{sr} f_{sr} \quad (2)$$

$$\eta_a = 0.25(3 + 2\bar{\lambda}) \quad (3)$$

$$\eta_c = 4.9 - 18.5\bar{\lambda} + 17\overline{\lambda^2} \quad (4)$$

$$\bar{\lambda} = \sqrt{N_{pl,Rk}/N_{cr}} \quad (5)$$

$$N_{pl,Rk} = A_s f_y + A_c f_{ck} + A_s f_{yr} \quad (6)$$

In these equations, N_{cr} is the elastic critical normal force for the relevant buckling mode.

2.3 Formulas by previous researchers

Richart *et al.* (1928) were the first to suggest a strength enhancement formula of concrete, presented here as Eq. (7), based on a triaxial compression test. The confined strength of concrete is increased by $k_1 f_l$ from the uniaxial compressive strength, where f_l is the lateral confining pressure and k_1 is the coefficient for lateral confinement. Later, Balmer *et al.* (1949) calibrated the coefficient k_1 as 5.6 on average based on an extensive experimental study. Saatcioglu *et al.* (1992) modified k_1 to $6.7(f_l)^{-0.17}$ and Razvi *et al.* (1999) modified $k_1 f_l$ to $6.7(f_l)^{0.83}$ based on their research.

$$f_{cc} = f_{ck} + k_1 f_l \quad (7)$$

Sun (2008), Liu *et al.* (2016), and O'Shea and Bridge (2000) developed design formulas for the ultimate compressive strength of CFTs considering the confinement effect, as shown in Table 2. As indicated in the table, Sun (2008) defined the strength using a simple multiplication of the concrete area by the confined strength of the concrete (f_{cc}) but did not include the steel tube strength in the formula. Instead, the strength enhancement was defined as a function of D/t, f_y, and f_{ck}. The formula by Liu *et al.* (2016) separately considered the contributions of the concrete and the steel tube. However, the yield strength of the steel tube was reduced to $0.61 f_y$, and their concrete strength enhancement formula uses a format identical to that by Richart *et al.* (1928) except that the lateral confining pressure was defined as a function of D/t and f_y. In the formula, the maximum lateral stress was assumed to be $0.54 f_y$. The reduction in the steel tube strength was determined based on experimental, theoretical and FEA results. It can be explained using the von-Mises yield criterion of steel subjected to multi-dimensional stresses. O'Shea and Bridge (2000) subdivided the concrete strength ranges into $f_{ck} \le 50\ MPa$ and $80\ MPa \le f_{ck} \le 100\ MPa$ in their estimation of the concrete strength enhancement.

3. Material models

3.1 Stress-strain model of confined concrete

According to Schneider *et al.* (1998), when the axial load is gradually applied to CFT, the confining pressure into concrete does not exist in the beginning of the loading

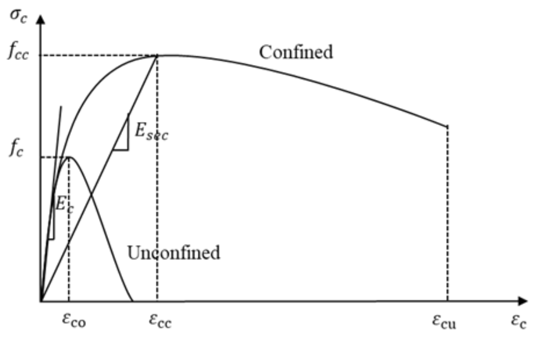

Fig. 2 Mander's confined concrete stress-strain curve

because the Poisson's ratio of concrete is smaller than that of steel. Under linear elastic strain range, the Poisson's ratios of concrete and steel are approximately 0.2 and 0.3, respectively. As the strain of concrete increases, number of micro cracks increase and crack width is widened, consequently, apparent volume increases. That is, the apparent Poisson's ratio of concrete can exceed the steel's ratio when the axial strain reaches near the peak point of stress-strain curve. Therefore, the concrete in CFT under uniaxial compression load will be subjected to triaxial stresses at the high nonlinear strain.

This paper is to predict the ultimate strength of a circular CFT, stress-strain model of concrete under compression considering confinement effect is required. In this paper, the stress-strain relationship of Eq. (8), as shown in Fig. 2 proposed by Mander *et al.* (1988a, 1988b), which considers the confinement effect by lateral reinforcement based on the Popovic's (1973) formula, was chosen for an analysis of the CFT section. In the formula, the concrete strength enhancement (f_{cc}) is expressed as a function of f_c and σ_{rc}; at the same time, the peak strain of confined concrete was increased based on Eq. (10).

$$\sigma_c = \frac{f_{cc} x r}{r - 1 + x^r} \tag{8}$$

$$f_{cc} = f_c\left(-1.254 + 2.254\sqrt{1 + \frac{7.94\sigma_{rc}}{f_c}} - \frac{2\sigma_{rc}}{f_c}\right) \tag{9}$$

$$\varepsilon_{cc} = 0.002\left(1 + 5\left(\frac{f_{cc}}{f_c} - 1\right)\right) \tag{10}$$

3.2 Failure criteria of concrete

In this paper, the failure criterion by Drucker and Prager (1952) based on a pressure-dependent model was used to judge the critical state of concrete under multi-axial pressure. The criterion has the form of Eq. (11), where I_1 and J_2 are correspondingly the first and second invariants of the Cauchy stress tensor, respectively expressed as Eqs. (12)-(13) for the concrete of the CFT. Here, σ_0, α, and β are concrete material properties that were determined experimentally (Chen 1982). In equation (12), σ_{11} is the longitudinal stress, σ_{22} and σ_{33} are identically acting confining stresses and are denoted here as σ_{rc}.

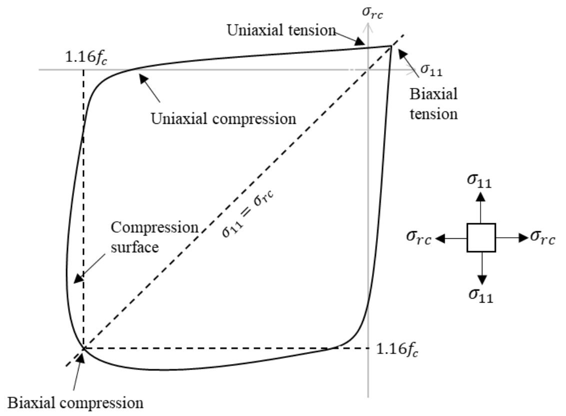

Fig. 3 Strength of concrete under biaxial stress

$$f(I_1, J_2) = [\alpha I_1 + 3\beta J_2]^{1/2} = \sigma_0 \tag{11}$$

$$I_1 = \sigma_{11} + \sigma_{22} + \sigma_{33} = \sigma_{11} + 2\sigma_{rc} \tag{12}$$

$$J_2 = \frac{1}{3}(\sigma_{11} - \sigma_{rc})^2 \tag{13}$$

During a uniaxial test, the concrete reaches the failure criterion when the maximum principal stress, σ_{11}, matches the uniaxial compressive strength of the concrete, f_c, becoming σ_0. Therefore, the simplified relationship between α and β can be expressed as Eq. (15). Under a biaxial test where σ_{11} is equal to the confining pressure, σ_{rc}, the maximum failure stress is approximately $1.16f_c$, as shown in Fig. 3, according to Kupfer *et al.* (1969). Thus, the additional relationship between α and β can be expressed as Eq. (17). By solving Eqs. (15)-(17) simultaneously, α and β can be determined as $-0.355f_c$ and 1.355, respectively. Finally, equation (11) can be substituted by Eq. (18).

$$f(I_1, J_2) = [\alpha f_c + \beta {f_c}^2]^{1/2} = f_c \tag{14}$$

$$\alpha = f_c - \beta f_c \tag{15}$$

$$f(I_1, J_2) = [\alpha(\sigma_{11} + \sigma_{rc}) + \beta\sigma_{11}^2]^{1/2} = \sigma_0 = f_c \tag{16}$$

$$\sigma_0 = [2.32\alpha f_c + 1.16^2\beta {f_c}^2]^{1/2} = f_c \tag{17}$$

$$\begin{gathered} f(I_1, J_2) = [\alpha(\sigma_{11} + 2\sigma_{rc}) + \beta(\sigma_{11} - \sigma_{rc})^2]^{1/2} = \sigma_0 \\ \alpha = -0.355f_c; \quad \beta = 1.355 \end{gathered} \tag{18}$$

3.3 Material model of steel tube and failure criterion

As the Poisson's ratio of concrete exceeds that of steel under high compressive stress, the concrete in the steel tube of a CFT begins to interact with the steel tube, pushing it outward. This results in hoop stress (σ_θ) in the steel tube. That is, the steel tube is subjected to multiaxial stresses. In contrast to the uniaxial yielding that occurs when the

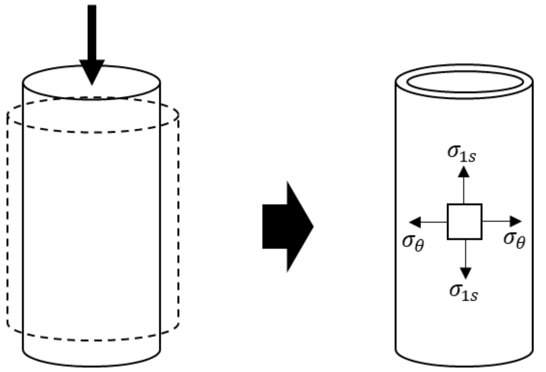

Fig. 4 Stress state of the steel tube

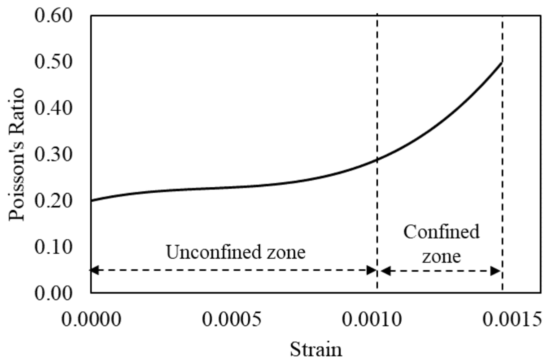

Fig. 5 Poisson's ratio and strain curve

uniaxial stress (σ_{1s}) reaches the yield stress of material, the steel tube as a ductile material begins to yield or lose elasticity when the equivalent von-Mises stress reaches the yield stress of the material (Chakrabarty 2006). Therefore, the steel tube can yield under stress lower than the yield stress of the material. This was also explained in studies by Furlong (1967) and Liu *et al.* (2016).

Considering that the stress in the thickness direction of the steel tube subjected to internal pressure is much lower than the hoop stress and considering that there is no shear in the tube, the tube can be assumed to be under principal plane stress, as indicated in Fig. 4 (He *et al.* 2019). This study also assumed principal plane stress of the steel tube and used the yield criterion of Eq. (19). Steel typically shows hardening behavior after yielding, but the behavior is highly dependent on the type and strength of the steel. (Hasan *et al.* 2019) Thus, a bilinear and perfect elasto-plastic model for steel is assumed in this paper.

$$\sigma_{1s}^2 - \sigma_{1s}\sigma_\theta + \sigma_\theta^2 \leq f_y^2 \tag{19}$$

3.4 Nonlinear poisson's ratio of concrete

Kupfer *et al.* (1969) proved that the Poisson's ratio of concrete is proportional to the concrete strain to some extent based on test results. Farooq *et al.* (2018) presented test results that showed that the Poisson's ratio of concrete can exceed 0.5 near the peak strain of the stress-strain curve and converge to approximately 0.4 as the axial strain increases after the peak point. Madas *et al.* (1992) suggested the relationship between the concrete axial strain and the Poisson's ratio of Eq. (20) and Fig. 5 based on a least squares fit using data from Kupfer *et al.* (1969). Eq. (20) gives a result that exceeds 0.5, but for a simple application, the maximum value was assumed to be 0.5 regardless of the strain. If the initial Poisson's ratio (v_{co}) is assumed to be 0.2, the strain for $v_c = 0.3$ when the Poisson's ratio of concrete equals that of steel is approximately 0.001. Therefore, concrete may begin to be confined from $\varepsilon_c = 0.001$. In another sense, the steel tube may begin to confine the concrete before the tube reaches the yielding point.

$$v_c = v_{co}\left(1 + 1.3763\frac{\varepsilon_c}{\varepsilon_{cc}} - 5.36\left(\frac{\varepsilon_c}{\varepsilon_{cc}}\right)^2 + 8.586\left(\frac{\varepsilon_c}{\varepsilon_{cc}}\right)^3\right) \tag{20}$$

4. Proposed procedure for calculating the maximum compressive strength of a CFT

As shown in Eqs. (1)-(2), the prediction formulas of AISC (2016) and Eurocode 4 (2004) do not directly consider the interaction between the concrete and steel tube. In addition, the formulas can only be applied for specified ranges of design variables such as the concrete compressive strength and yield strength of steel. In this study, the stress-strain relationships of the concrete and steel tube and the Poisson's ratio-strain relationship of the concrete are directly used and constitutive equations are constructed based on the force equilibrium and strain compatibility. Therefore, an accurate estimation of the compressive strength of a CFT can be achieved for wider ranges of the concrete compressive strength and yield strength of steel. Nevertheless, for simplicity, the following assumptions are adopted.

1) The cross-section of the CFT is subjected to uniform axial strain without eccentricity.
2) The concrete and the steel tube behave monolithically without any gap between the two materials.
3) The compressive strength of the CFT is reached when the von-Mises stress of the steel tube and the combined stress of the concrete reach the yield stress of the steel and/or the failure stress of the biaxial interaction diagram of the concrete, respectively.

4.1. Construction of an equilibrium equation

When the Poisson's ratios of the concrete and steel tube become equal, the interaction begins. Assuming that the coordinate axes of the radial and circumferential directions are correspondingly r and θ, the compression on the concrete, $(D-2t)\sigma_{rc}$, is equilibrated by the tension on the steel tube, $2t\sigma_\theta$, as shown in Fig. 6. Here, σ_{rc} and σ_θ denote the confinement stress in the concrete and the hoop stress in the tube, respectively.

Deformations and stresses in the concrete and steel tubes of CFTs can be determined based on the superposition method, as shown in Fig. 6. If monolithic behavior of the concrete and the tube is assumed, the deformation of concrete in the radial direction, $u_{1c} + u_{2c}$, should be

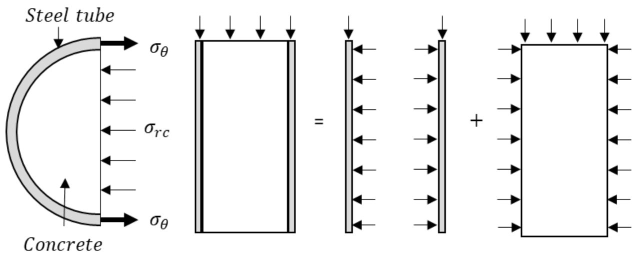

Fig. 6 Confined stress in a concrete-filled steel tube

identical to the deformation of the steel tube, $u_{1s}+u_{2s}$. u_{1c} and u_{1s} are correspondingly the radial strains in the concrete and the steel tube due to the Poisson's ratios under uniaxial compression and are expressed respectively as Eqs. (22)-(23). In addition, u_{2c} and u_{2s} are likewise the radial strains in the concrete and steel tube due to confining pressure and are expressed as Eqs. (24)-(25) based on elasticity theory (Sadd 2004, Yu *et al.* 2010).

$$u_{1c}=r_{oc}\varepsilon_{rc}=-r_{oc}v_c\varepsilon_z \tag{22}$$

$$u_{1s}=r_{os}\varepsilon_{rs}=-r_{os}v_s\varepsilon_z \tag{23}$$

Here, ε_z is the compressive strain in the longitudinal direction, and ε_{rc} and ε_{rs} are the strains in the concrete and steel tube in the radial direction, respectively. v_c and v_s are the Poisson's ratios of the concrete and steel, respectively, and r_{oc} and r_{os} are likewise the initial radii of the concrete and the tube.

$$u_{2c}=\frac{\sigma_{rc}(v_c^2-1)}{E_c}\left(1-\frac{v_c}{1-v_C}\right)\left(\frac{D-2t}{2}\right) \tag{24}$$

$$u_{2s}=\frac{(D-2t)\,\sigma_{rc}(1+v_s)}{8E_st(t-D)}[D^2+(1-2v_s)(D-2t)^2] \tag{25}$$

Finally, the confining pressure on the concrete, σ_{rc}, can be expressed as a function of $D, t, v_c, v_s, \varepsilon_z, E_c,$ and E_s, as shown in Eq. (26), by combining equations (22) to (25).

$$\sigma_{rc}=\frac{-\varepsilon_z(v_S-v_c)}{\frac{1+v_s}{4tE_s(D-t)}[D^2+(1-2v_s)(D-2t)^2]-\frac{(1+v_c)(1-2v_c)}{E_c}} \tag{26}$$

4.2. Proposed procedure

A new procedure (referred to as Kim's procedure) that directly uses the stress-strain relationships of the concrete and steel tube and the Poisson's ratio-strain relationship of concrete in order to provide an accurate estimation of the circular CFT compressive strength and for wide range of design variables is presented as a flowchart in Fig. 7.

(1) Initialize variables $N_i=0$ $(i=0)$
(2) The axial strain (ε_z) of concrete when $v_c=v_s$ is initially computed and the strain is slightly increased, $\varepsilon_z=\varepsilon_z+\Delta\varepsilon_z$.
(3) The Poisson's ratio is determined at the axial strain using Eq. (20).
(4) The confining stress on concrete (σ_{rc}) is calculated by Eq. (26).
(5) The hoop stress and the axial stress of the steel tube are calculated at the given strain, and the combined stress of the steel tube is calculated by the von-Mises stress equation to assess whether the steel reaches the yield criterion.
(6) If the combined stress of the steel tube is yielded, σ_{1s} and σ_θ are determined using the σ'_{1s} and σ'_θ values respectively when the condition of $f_2(\sigma'_{1s},\sigma'_\theta)=f_y$ is satisfied.
(7) If the combined stress of steel tube is determined, the confining stress of the concrete is limited to σ'_{rc} and the confining stress of the concrete is determined to be equal to the smaller value between σ_{rc} and σ'_{rc}.
(8) The maximum confined strength and strain of the concrete are respectively calculated by Eq. (9) and Eq. (10), and the stress-strain relationship of the confined concrete is determined using Eq. (8).
(9) The concrete axial stress, σ_c (or σ_{11}), is computed at the given strain and the combined stress of concrete is calculated to check if the concrete reaches the failure criterion.
(10) When the combined stress of the concrete reaches the failure criterion or the combined stress of the steel reaches the yield criterion, the compressive strength of the CFT is calculated via $N=\sigma_{1s}A_s+\sigma_cA_c$.
(11) When the calculated compressive strength of CFT(N_i) is less than or equal to N_{i-1}, the loop is stopped and the larger value between N_i and N_{i-1} is determined as the ultimate compressive strength of CFT.

5. Comparison with experiment results

5.1. Comparison with experimental results

In order to verify the prediction capabilities of Kim's procedure, 99 test data instances were collected from studies by Schneider *et al.* (1998), Kato (1955), Tomii *et al.* (1977), Saisho *et al.* (1999), Han *et al.* (2001), Huang *et al.* (2002), Yamamoto *et al.* (2002), Giakoumelis *et al.* (2004), Sakino and Hayashi (2004a, 2004b), and Li *et al.* (2005). All of the specimens are short and round CFT and have compact sections such that the confinement effect is active in all cases. The variables of the specimens were the compressive strength of the concrete, the yield strength of the steel tube, and the diameter and thickness of the tube. The data are listed in Table 3. The range of the compressive strength of concrete is from 18.1 MPa to 107.3 MPa, and the range of the yield strength of the steel tube is from 249 MPa to 843 MPa. D/t ranges from 17 to 75. Though the range of D/t is relatively wide, all values fall in the compact section category. The data distributions for each of the variables are presented in Fig. 8.

In Table 3, the predictions by AISC (2016), Eurocode 4 (2004), Liu *et al.* (2016) are compared with those by Kim's procedure. The average ratios of the test data to the

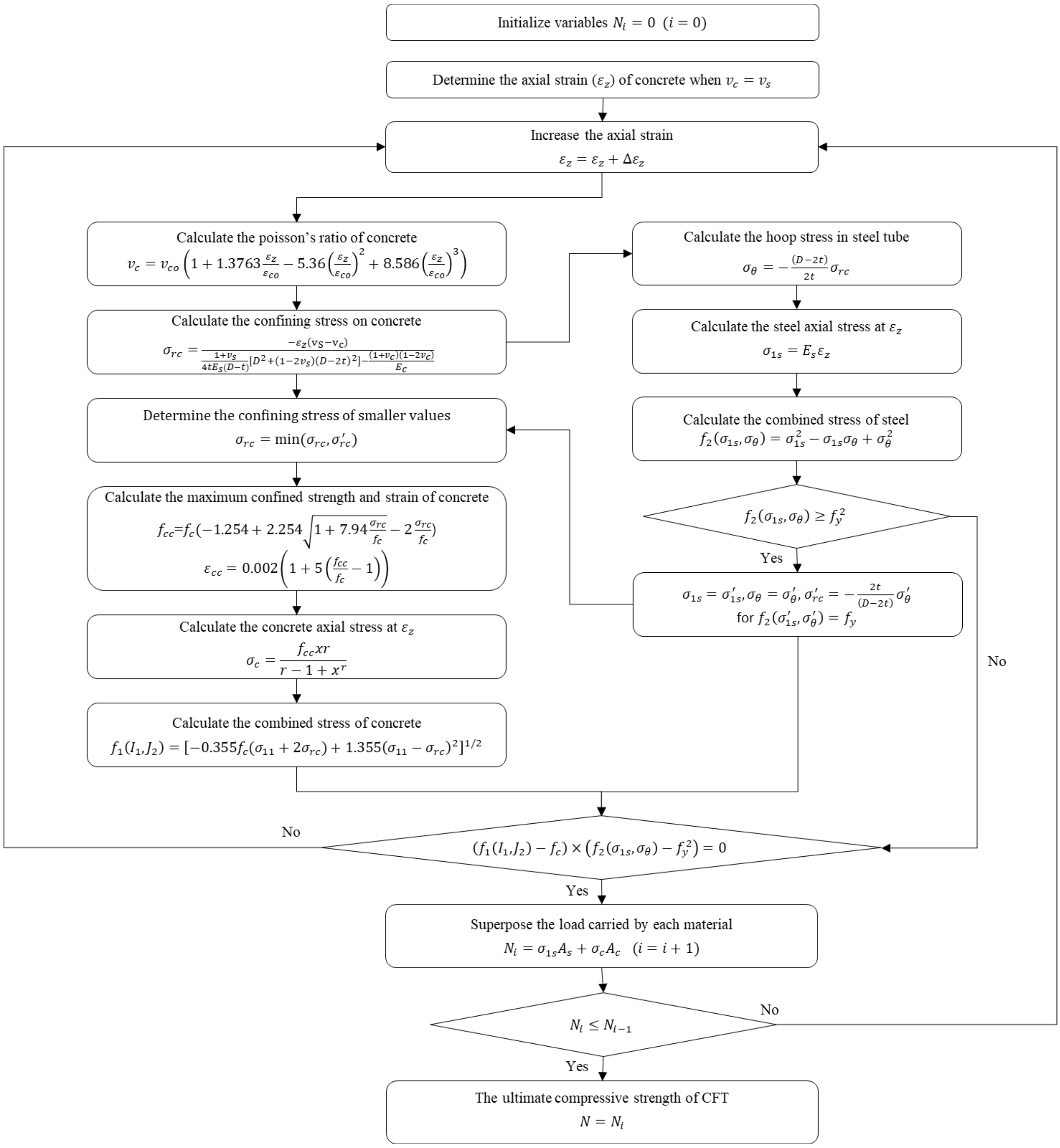

Fig. 7 Kim's procedure to predict the ultimate compressive strength of circular CFTs

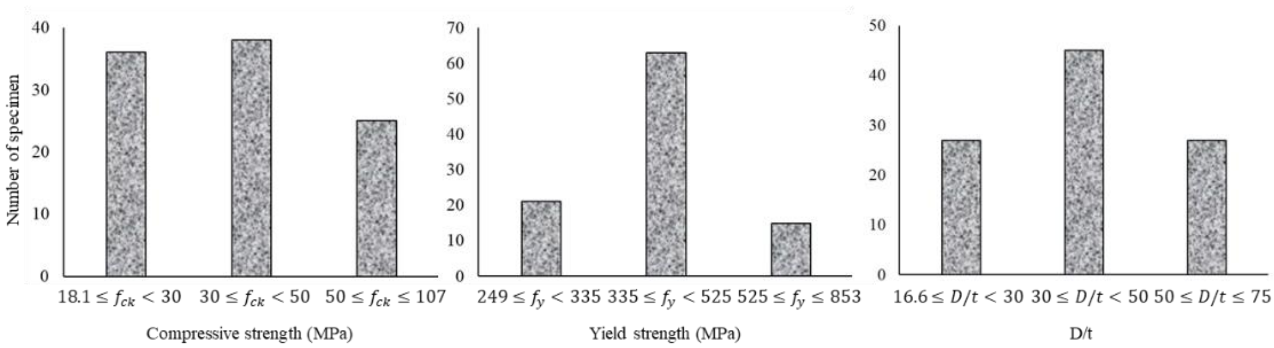

Fig. 8 Classification of specimens according to the design variables

Table 3 Experimental data of the concrete-filled steel tube

Ref.		D (mm)	t (mm)	D/t	f_y (MPa)	f_{ck} (MPa)	N_{exp} (kN)	Kims'	AISC (2016)	EC4 (2004)	Liu *et al.* (2016)
								N_{exp}/N_{cal}	N_{exp}/N_{cal}	N_{exp}/N_{cal}	N_{exp}/N_{cal}
Schneider *et al.* (1998)	C1	141	3	47	285	28.2	881	1.03	1.10	0.83	0.80
	C2	141	6.5	22	313	23.8	1344	0.99	1.05	0.78	0.69
Kato (1955)	C04LB	300	4.5	67	389	28.3	3930	1.07	1.10	0.76	0.81
	C06LB	300	5.7	53	408	28.3	4630	1.05	1.12	0.75	0.80
	C08LB	300	7.7	39	392	28.3	5020	1.00	1.04	0.68	0.72
	C12LB	300	11.9	25	355	28.3	6030	0.97	1.00	0.64	0.68
	C04MB	300	4.5	67	389	36.3	4640	1.07	1.13	0.81	0.86
	C06MB	300	5.7	53	408	33	5230	1.14	1.18	0.80	0.85
	C08MB	300	7.7	39	392	36.2	5940	1.07	1.11	0.75	0.79
	C12MB	300	11.9	25	355	36.3	7370	1.09	1.12	0.73	0.78
	C06HB	300	5.7	53	408	84.1	8100	1.00	1.03	0.80	0.83
	C08HB	300	7.7	39	392	84.1	8560	0.98	1.00	0.76	0.79
	C04MF	200	4.8	42	447	107.3	4310	0.97	0.95	0.76	0.76
	C06MF	200	6	33	391	107.3	4660	0.98	0.99	0.79	0.79
	C09MF	200	8.4	24	371	107.3	5670	1.10	1.09	0.85	0.84
	C04MU	200	4.8	42	447	75.1	3360	0.96	0.93	0.72	0.72
	C06MU	200	6	33	391	75.1	3820	1.00	1.02	0.78	0.78
	C08MU	200	8.4	24	371	75.1	5050	1.18	1.19	0.89	0.87
Tomii *et al.* (1977)	4HN	150	4	38	280	28.7	1118	1.02	1.10	0.82	0.79
	3MN	150	3.2	47	290	22	865	1.01	1.07	0.78	0.76
	4MN	150	4	38	280	22	992	1.01	1.10	0.79	0.76
	2LN	150	2	75	337	18.1	700	1.01	1.13	0.82	0.81
	4LN	150	4	38	280	18.1	1100	1.21	1.31	0.93	0.89
Saisho *et al.* (1999)	H-30.1	101.6	2.99	34	377	59.9	921	1.11	1.21	1.01	0.92
	H-30.2	101.6	2.99	34	377	59.9	921	1.11	1.21	1.01	0.92
	H-30.3	101.6	2.96	34	377	59.9	901	1.06	1.19	1.00	0.90
	H-50.1	139.8	2.78	50	341	55	1323	1.06	1.15	0.93	0.91
	H-50.2	139.8	2.78	50	341	55	1391	1.09	1.21	0.98	0.95
	H-50.3	139.8	2.78	50	341	55	1313	1.01	1.14	0.92	0.90
	H-60.1	139.8	2.37	59	463	59.9	1558	1.10	1.21	0.97	0.94
	H-60.2	139.8	2.37	59	463	68	1577	1.03	1.13	0.92	0.89
	H-60.3	139.8	2.37	59	463	68	1577	1.03	1.13	0.92	0.89
	H-60.4	139.8	2.37	59	463	68	1626	1.07	1.16	0.95	0.92
	L-30.1	101.6	2.96	34	377	24.4	676	1.16	1.29	1.05	0.91
	L-30.2	101.6	2.99	34	377	26.6	715	1.19	1.32	1.08	0.93
	L-30.3	101.6	2.99	34	377	28.2	715	1.16	1.30	1.06	0.92
	L-50.1	139.8	2.78	50	341	24.4	931	1.13	1.25	0.93	0.91

predictions show that Kim's procedure predicts the ultimate strength more accurately than the other methods. The average ratio by Kim's method is 1.09 with a standard deviation of 0.08. AISC (2016) and EC4 (2004) show average ratios of 1.16 and 0.88 with standard deviations of 0.10 and 0.11, respectively. That is, AISC (2016) may underestimate the strength by approximately 16% on average, but EC4 (2004) may overestimate the strength by nearly 12% on average. Liu *et al.* (2016) show an average ratio of 0.84 with a standard deviation of 0.09. This indicates that the model by Liu *et al.* (2016) can overestimate the strength by more than 15% on average.

Table 3 Continued

Ref.		D (mm)	t (mm)	D/t	f_y (MPa)	f_{ck} (MPa)	N_{exp} (kN)	Kims' N_{exp}/N_{cal}	AISC (2016) N_{exp}/N_{cal}	EC4 (2004) N_{exp}/N_{cal}	Liu *et al.* (2016) N_{exp}/N_{cal}
Han *et al.* (2001)	Sp1	159	5	32	390	36.6	2040	1.17	1.21	0.89	0.84
	Sp2	319	7.9	40	358	47.5	7000	1.04	1.08	0.76	0.80
	Sp3	165	2.8	59	363	48.3	1662	1.05	1.10	0.86	0.86
	Sp4	204	6.1	33	389	22.9	2462	1.03	1.09	0.73	0.73
	Sp5	204	6.3	32	405	29.9	2932	1.08	1.13	0.77	0.77
	Sp6	121	3.7	33	295	21.1	695	0.99	1.07	0.81	0.72
Huang *et al.* (2002)	CU-040	200	5	40	266	27.2	1694	0.94	1.02	0.72	0.74
Yamamoto *et al.* (2002)	C10A-2A-1	101.4	3.02	34	371	22.3	660	1.17	1.30	1.05	0.91
	C10A-2A-2	101.9	3.07	33	371	22.3	649	1.13	1.26	1.02	0.87
	C10A-2A-3	101.8	3.05	33	371	22.3	682	1.15	1.33	1.08	0.92
	C10A-3A-1	101.7	3.04	33	371	38.6	800	1.15	1.29	1.06	0.94
	C10A-3A-2	101.3	3.03	33	371	38.6	742	1.08	1.20	0.99	0.88
	C10A-4A-1	101.9	3.04	34	371	49.2	877	1.13	1.26	1.05	0.94
	C10A-4A-2	101.5	3.05	33	371	49.2	862	1.14	1.25	1.04	0.93
Giakoumelis *et al.* (2004)	C3	114.4	3.98	29	343	25.1	826	1.06	1.17	0.93	0.83
	C4	114.6	3.99	29	343	78.1	1308	1.02	1.14	0.95	0.89
	C7	114.9	4.91	23	365	27.9	1050	1.08	1.18	0.96	0.85
	C8	115	4.92	23	365	87.7	1787	1.17	1.31	1.10	1.02
	C9	115	5.02	23	365	47.4	1390	1.18	1.31	1.08	0.98
Sakino and Hayashi (2004a)	L-20-1	178	9	20	283	22.6	2120	0.97	1.11	0.81	0.82
	L-20-2	178	9	20	283	22.6	2060	0.94	1.08	0.79	0.79
	H-20-1	178	9	20	283	46.3	2720	1.02	1.16	0.87	0.89
	H-20-2	178	9	20	283	46.3	2730	1.05	1.16	0.88	0.89
	L-32-1	179	5.5	33	249	22.6	1410	0.98	1.12	0.80	0.82
	L-32-2	179	5.5	33	249	24.4	1560	1.06	1.20	0.86	0.88
	H-32-1	179	5.5	33	249	44.5	2080	1.07	1.21	0.93	0.94
	H-32-2	179	5.5	33	249	44.5	2070	1.06	1.21	0.92	0.94
	L-58-1	174	3	58	266	24.4	1220	1.14	1.28	0.95	0.97
	L-58-2	174	3	58	266	24.4	1220	1.14	1.28	0.95	0.97
	H-58-1	174	3	58	266	46.6	1640	1.04	1.16	0.93	0.94
	H-58-2	174	3	58	266	46.6	1710	1.08	1.21	0.97	0.98
Sakino and Hayashi (2004b)	CC4A2	149	3	50	308	25.4	941	1.00	1.10	0.81	0.79
	CC6A2	122	4.5	27	576	25.4	1509	1.22	1.17	0.94	0.75
	CC6A41	122	4.5	27	576	40.5	1657	1.18	1.14	0.91	0.75
	CC6A42	122	4.5	27	576	40.5	1663	1.14	1.15	0.91	0.76
	CC6A8	122	4.5	27	576	77	2100	1.12	1.13	0.93	0.80
	CC6C2	239	4.5	53	507	25.4	3035	1.08	1.08	0.72	0.74

More detailed analyses of the better performance by Kim's method are presented in the next chapter.

5.2 Performance evaluation of the proposed procedure

Fig. 9 presents a comparison of the ultimate strength from various prediction models compared to the experimental results. Figs. 9(a)-9(c) show the distribution of N_{exp}/N_{cal} according to the compressive strength of concrete. Kim's procedure shows overall good agreement with the experimental results in all ranges of the compressive strength of concrete. The data distributions from the yield strength of the steel tube and D/t are shown in Figs. 9(d)-9(f) and in Figs. 9(g)-9(i), respectively. Kim's procedure shows ultimate strength outcomes similar to

Table 3 Continued

Ref.		D (mm)	t (mm)	D/t	f_y (MPa)	f_{ck} (MPa)	N_{exp} (kN)	Kims' N_{exp}/N_{cal}	AISC (2016) N_{exp}/N_{cal}	EC4 (2004) N_{exp}/N_{cal}	Liu *et al.* (2016) N_{exp}/N_{cal}
Sakino and Hayashi (2004b)	CC6C41	239	4.5	53	507	40.5	3583	1.04	1.04	0.73	0.75
	CC6C8	239	4.5	53	507	77	5578	1.09	1.11	0.85	0.87
	CC8A2	108	6.5	17	853	25.4	2275	1.15	1.08	1.02	0.64
	CC8A42	108	6.5	17	853	40.5	2402	1.14	1.07	0.98	0.65
	CC8A8	108	6.5	17	853	77	2713	1.09	1.05	0.95	0.68
	CC8C2	222	6.5	34	843	25.4	4964	1.00	1.03	0.69	0.65
	CC8C41	222	6.5	34	843	40.5	5638	1.00	1.05	0.71	0.69
	CC8C42	222	6.5	34	843	40.5	5714	1.02	1.06	0.72	0.70
	CC8C8	222	6.5	34	843	77	7304	1.05	1.09	0.78	0.76
	CC8D2	324	6.5	50	823	25.4	10045	1.25	1.34	0.82	0.87
	CC8D41	324	6.5	50	823	41.1	11044	1.11	1.26	0.81	0.86
	CC8D42	324	6.5	50	823	41.1	11044	1.17	1.26	0.81	0.86
	CC8D8	324	6.5	50	823	85.1	13849	1.05	1.14	0.80	0.84
Li *et al.* (2005)	sc-1	156.4	3.8	41	342	30.5	1650	1.30	1.37	1.01	0.98
	sc-2	156.4	3.8	41	342	30.5	1710	1.34	1.42	1.05	1.01
	sc-3	156.4	3.8	41	342	30.5	1600	1.26	1.33	0.98	0.95
	sc-4	149.4	4.8	31	366	30.5	1600	1.15	1.19	0.87	0.81
	sc-5	149.4	4.8	31	366	30.5	1700	1.18	1.26	0.93	0.86
	sc-6	149.4	4.8	31	366	30.5	1600	1.13	1.19	0.87	0.81
	sc-7	148.6	5.2	29	379	30.5	1800	1.21	1.25	0.92	0.85
	sc-8	148.6	5.2	29	379	30.5	1850	1.23	1.28	0.95	0.87
	sc-9	148.6	5.2	29	379	30.5	1700	1.13	1.18	0.87	0.80
	sc-10	146.4	6.3	23	360	30.5	2000	1.23	1.28	0.95	0.86
	sc-11	146.4	6.3	23	360	30.5	1950	1.20	1.25	0.93	0.84
	sc-12	146.4	6.3	23	360	30.5	2100	1.29	1.35	1.00	0.90
Average								1.09	1.16	0.88	0.84
Standard deviation								0.08	0.10	0.11	0.09

those in experiment results when $249\ \text{MPa} \leq f_y \leq 525\ \text{MPa}$ and $16.6 \leq D/t \leq 50$.

However, Kim's procedure tends to underestimate the ultimate strength of the CFT compared to the experimental results when the yield strength of the steel tube exceeds 525 MPa or when D/t is greater than 50 (in Figs. 9(f) and 9(i)). This difference increases to nearly 20% in high-strength specimens, which have ultimate strength levels what exceed 10000 kN. According to the experimental conditions above, the yield strength of the steel tube is high, but the confinement effect on the concrete is relatively weak because the thickness of the steel tube is relatively thin. When predicting the ultimate strength of a CFT, Kim's procedure superimposes the strength calculated from the stresses of the two materials at the moment of concrete failure or steel tube yield. Because the strength of concrete is much lower than that of the steel tube in the above conditions, the strength of concrete is the governing factor when calculating the ultimate strength according to the algorithm. In other words, in the case of a specimen with a yield strength of 525 MPa or more, (a specimen with considerably higher yield strength compared to the compressive strength of concrete), the steel tube reaches the yield strength long after the concrete has reached its failure. In these cases, it can be considered that the steel tube can actually take more of a load after concrete failure compared to the strength as calculated by Kim's procedure. Nevertheless, even under these specific conditions, Kim's procedure provides a result closer to the ultimate strength in the experimental results than the other prediction models.

In order to evaluate the accuracy of each prediction model objectively, N_{exp}/N_{cal}, RMSE, RMSLE, and R^2 were calculated as a performance index. Table 4 shows a performance index comparing the ultimate strength of a CFT as obtained from Kim's procedure, AISC (2016), Eurocode 4 (2004), and the formula suggested by Liu *et al.* (2016) with the experimental results. Table 5 shows the average of each performance index for all test specimens. All performance indexes show that Kim's procedure has the smallest differences from the experimental results compared

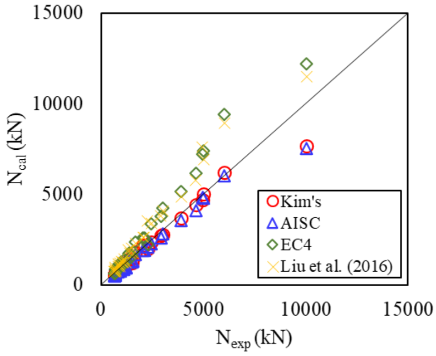

(a) 18.1 MPa $\leq f_{ck} <$ 30 MPa

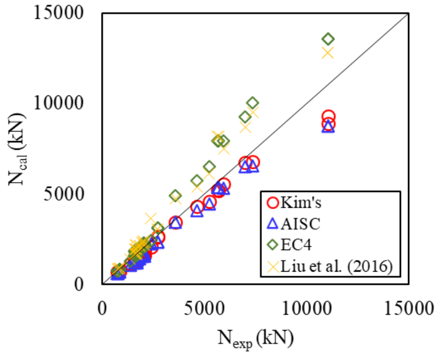

(b) 30 MPa $\leq f_{ck} <$ 50 MPa

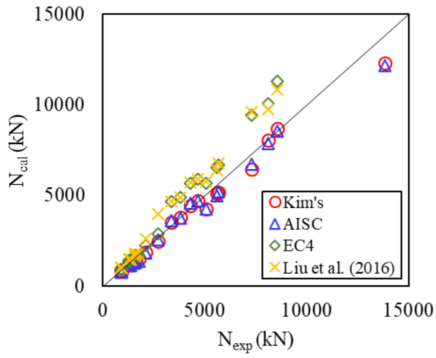

(c) 50 MPa $\leq f_{ck} <$ 107 MPa

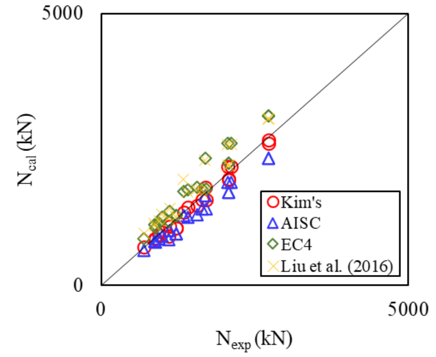

(d) 249 MPa $\leq f_y <$ 335 MPa

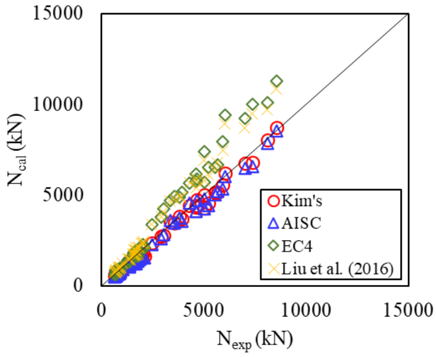

(e) 335 MPa $\leq f_y <$ 525 MPa

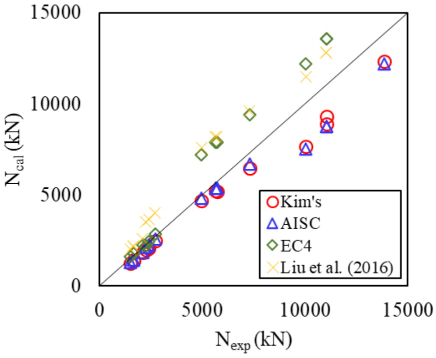

(f) 525 MPa $\leq f_y <$ 853 MPa

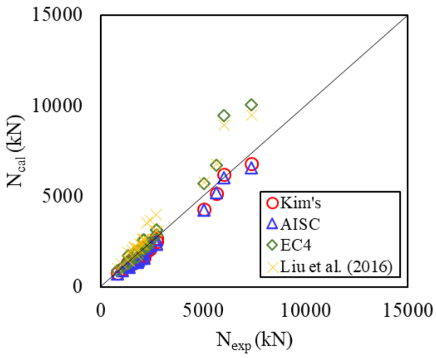

(g) 16.6 $\leq D/t <$ 30

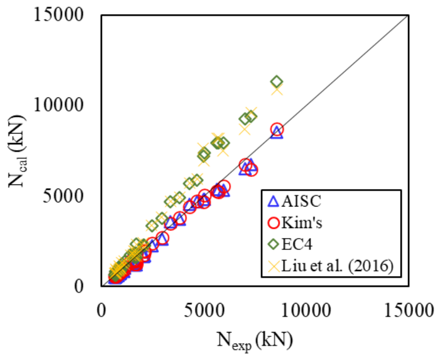

(h) 30 $\leq D/t <$ 50

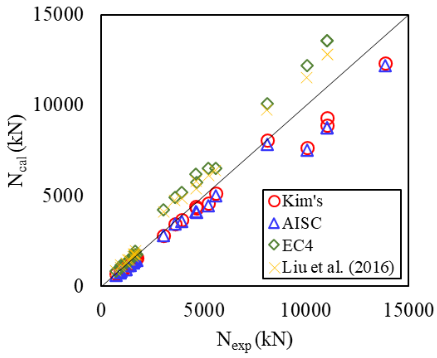

(i) 50 $\leq D/t <$ 75

Fig. 9 Distribution of the experimental data and calculated results

to the other models. According to the performance index of N_{exp}/N_{cal}, Kim's procedure and AISC (2016) tend to underestimate the ultimate strength of CFT, and EC4 (2004) and the method by Liu *et al.* (2016) tend to overestimate this measure. AISC (2016) greatly underestimates the ultimate strength because it cannot sufficiently consider the confinement effect on the concrete. Although Eurocode 4 (2004) considers the confinement effect on the concrete using the strength factor, the ultimate strength of the composite section is overestimated because this method assumes that the steel tube behaves in an elastic region until the maximum compressive strain of the concrete.

Regarding the RMSE and RMSLE results, which can directly compare the absolute deviation of the prediction results, Kim's procedure shows the best results among the prediction models. Kims' procedure is possible to accurately calculate the ultimate strength of CFT because it considers the confinement effect and the non-linear Poisson's ratio of the concrete appropriately. In addition, the high reliability of proposed process compared to other prediction models suggests that the above factors should be considered in detail for each load level..

6. Conclusions

In this study, in order to predict the composite structural behavior of a circular CFT under multiaxial stress accurately, a procedure that estimates the ultimate compressive strength of a CFT considering the confinement effect and the nonlinear Poisson's ratio of concrete is proposed. The failure stress of a biaxial interaction diagram

Table 4 Comparison of performance indexes from each prediction model

Performance index	Compressive strength				Yield strength				Diameter thickness ratio			
	Kims'	AISC (2016)	EC4 (2004)	Liu *et al.* (2016)	Kims'	AISC (2016)	EC4 (2004)	Liu *et al.* (2016)	Kims'	AISC (2016)	EC4 (2004)	Liu *et al.* (2016)
	f_{ck} < 30MPa				f_y < 335MPa				D/t < 30			
N_{exp}/N_{cal}	**1.07**	1.16	0.86	0.81	**1.04**	1.17	0.88	0.95	1.12	1.16	**0.91**	0.81
RMSE	**358**	463	993	914	**96**	260	278	319	**307**	331	899	913
RMSLE	**0.04**	0.07	0.09	0.11	**0.03**	0.08	0.07	0.09	**0.06**	0.07	0.07	0.10
R^2	**0.979**	0.974	**0.979**	0.965	**0.978**	0.973	0.952	0.931	0.984	**0.989**	0.966	0.974
	30 MPa≤ f_{ck}< 50 Mpa				335 MPa≤ f_y< 525 MPa				30 ≤ D/t < 50			
N_{exp}/N_{cal}	1.13	1.20	**0.90**	0.84	**1.10**	1.17	**0.90**	0.86	**1.09**	1.17	0.88	0.86
RMSE	**416**	647	1081	1044	**256**	335	1057	876	**173**	290	1054	977
RMSLE	**0.06**	0.09	0.07	0.09	**0.05**	0.08	0.08	0.08	**0.05**	0.08	0.09	0.08
R^2	**0.993**	0.986	0.991	0.988	**0.992**	0.990	0.985	0.988	**0.996**	0.992	0.991	0.984
	50 MPa ≤ f_{ck}				525 MPa ≤ f_y				50 ≤ D/t			
N_{exp}/N_{cal}	**1.06**	1.12	0.89	0.87	**1.11**	1.12	0.84	0.75	**1.08**	1.16	0.86	0.86
RMSE	**283**	451	1201	960	**769**	1075	1708	1752	**587**	903	1274	1116
RMSLE	**0.03**	0.06	0.07	0.07	**0.05**	0.06	0.10	0.13	**0.04**	0.07	0.08	0.08
R^2	0.995	0.990	0.995	**0.997**	0.987	0.982	**0.990**	0.982	0.992	0.987	**0.997**	0.992

Table 5 Performance index average

Performance index	Average			
	Kims'	AISC (2016)	EC4 (2004)	Liu *et al.* (2016)
N_{exp}/N_{cal}	1.09	1.16	0.88	0.84
RMSE	365	528	1061	987
RMSLE	0.05	0.07	0.08	0.09
R^2	0.989	0.983	0.989	0.984

of concrete and the von-Mises failure yield criterion were used to consider multi-dimensional stresses acting on the concrete and the steel tube, respectively. The proposed procedure, referred to as Kim's procedure, and the corresponding steps are as follows. The procedure initially computed the axial strain (ε_z) of concrete when $v_c = v_s$, with the strain slightly increased. The Poisson's ratio, confining the stress on the concrete and the stresses of the steel tube, is calculated at the given strain. Then, the combined stress of the steel tube is calculated by the von-Mises stress formula to check if the steel tube reaches the yield criterion. Once the combined stress of the steel tube is determined, the confining stress on the concrete is determined and the maximum confined strength and strain of the concrete is calculated by Mander's formula. The combined stress of the concrete is then calculated to check if the concrete reaches the failure criterion. If the combined stress of concrete reaches the failure criterion or the combined stress of the steel tube reaches the yield criterion, the compressive strength of the CFT is computed based on the superposition of the axial strengths of the concrete and steel tube. When the calculated compressive strength of the CFT (N_i) is less than or equal to N_{i-1}, the loop is stopped and N_i is determined as the ultimate compressive strength of the CFT. To evaluate the results of Kim's procedure, various experimental results and the prediction models by AISC (2016) and Eurocode 4 (2004) are compared. Performance indexes are used to evaluate the accuracy of the prediction models. The ultimate strength of the CFT by Kim's procedure is underestimated by about 9% on average compared to the experimental results. The RMSE and RMSLE outcomes according to Kim's procedure are 365 and 0.05, respectively. These evaluation values show that Kim's procedure has higher accuracy and greater reliability than the other prediction models tested here. However, when the strength of confined concrete is significantly lower than that of the steel tube, the differences between Kim's procedure and the experimental results increase to nearly approximately 20%. An improved model considering the difference in the strength between the steel tube and concrete should be addressed in an upcoming study.

Acknowledgments

This work is supported by the Korea Agency for Infrastructure Technology Advancement(KAIA) grant funded by the Ministry of Land, Infrastructure and Transport (Grant 21CTAP-C163558-01).

References

ACI 318 (2019), *Building Code Requirements for Strucural Concrete and Commentray*, American Concrete Institue, Farmington Hills, MI, USA.

ANSI/AISC 360 (2016), *Specification for Structural Steel Buildings*, American Institute of Steel Construction, Chicago, Illinois, USA.

Balmer, G.G. (1949), "Shearing strength of concrete under high triaxial stress - computation of mohr's envelope as a curve", *Structural Research Laboratory Report No. SP-23*, Office of Chief Engineer, Bureau of Reclamation, United States.

Chakrabarty, J. (2006), *Theory of Plasticity*, Amsterdam, Netherlands: Elsevier.

Chen, J., Liu, X., Liu, H. and Zeng, L. (2018), "Axial compression behavior of circular recycled concrete-filled steel tubular short columns reinforced by silica fume and steel fiber", *J. Steel Compos. Struct*., **27**(2), 193-200. https://doi.org/10.12989/scs.2018.27.2.193.

Chen, W.F. (1982), *Plasticity in Reinforced Concrete*, New York, NY: McGraw-Hill Book.

Drucker, D.C. and Prager, W. (1952), "Soil mechanics and plastic analysis on limit design", *J. Applied Math*., **10**(2), 157-165.

Eurocode 4 (2004), *Design of composite steel and concrete structures, Part 1-1: General rules and rules for buildings*, European Committee for Standardization, Brussels, Belgium.

Fan, J., Lyu, F., Ding, F., Bu, D., Wang, S., Tan, Z. and Tan, S. (2021), "Compatibility Optimal Design of Axially Loaded Circular Concrete-Filled Steel Tube Stub Columns", *J. Mater*., **14**(17), 4839. https://doi.org/10.3390/ma14174839.

Farooq, H., Mehmood, H., Malik, M.S. Hanif, A. (2018), *Effect of Steel Confinement on Axially Loaded Short Concrete Columns*, IOP Conf. Series: Materials Science and Engineering, 012026. https://10.1088/1757-899X/414/1/012026

Furlong, R.W. (1967), "Strength of steel-encased concrete beam columns", *J. Struct. Div*., **93**(5), 113-124. https://doi.org/10.12989/scs.2001.1.4.393.

Giakoumelis, G. and Lam, D. (2004), "Axial capacity of circular concrete-filled tube columns", *J. Constr. Steel Res*., **60**(7), 1049-1068. http://hdl.handle.net/10454/5652.

Han, L.H., Zhao, X.L. and Tao, Z. (2001), "Tests and mechanics model for concrete-filled SHS stub columns, columns and beam-columns", *J. Steel Compos. Struct*., **1**(1), 51-74https://doi.org/10.12989/scs.2001.1.1.051.

Hasan, H.G., Ekmekyapar, T. and Shehab, B.A. (2019), "Mechanical performances of stiffened and reinforced concrete-filled steel tubes under axial compression", *J. Marine Struct*., **65**.

Hasan, H.G. and Ekmekyapar, T. (2019), "Mechanical performance of stiffened concrete filled double skin steel tubular stub columns under axial compression", *J. Civil Eng*., **23**(5).

He, L., Lin, S. and Jinag, H. (2019), "Confinment effect of concrete-filled steel tube columns with infill concrete of different strength grades", *J. Front Matr*., **6**. https://doi.org/10.3389/fmats.2019.00071.

Huang, C.S., Yeh, Y.K., Liu, G.Y., Hu, H.T., Tsai, K.C., Weng, Y.T., Wang, S.H. and Wu, M.H. (2002), "Axial load behavior of stiffened concrete-filled steel columns", *J. Struct. Eng.*, **128**(9), 1222-1230. https://doi.org/10.1061/(ASCE)0733-45(2002)128:9(1222).

Kato, B. (1955), "Compressive strength and deformation capacity of concrete-filled tubular stub columns", *J. Struct. Constr. Eng AIJ*., 183-191.

Knowles, R.B. and Park, R. (1969), "Strength of concrete filled steel tubular columns", *J. Struct. Div*., **95,** 2565-2587.

Kupfer, H., Hilsdorf, H.K. and Rüsch, H. (1969), "Behavior of concrete under biaxial stresses", *J. ACI*., **66**, 656-666.

Li, B. and Hao, R.X. (2005), "The analysis of concrete filled steel tube column carrying capacity", *J. Baotou Univ Iron Steel Technol*., **24**, 5-8.

Liu, J., Zhou, X. and Gan, D. (2016), "Effect of friction on axially loaded stub circular tubed columns", *Adv. Struct. Eng*., **19**(3), 546-559. https://doi.org/10.1177/1369433216630125.

Luat, N.V., Shin, J., Han, S.W., Nguyen, N.V. and Lee, K. (2021), "Ultimate axial capacity prediction of CCFST columns using hybrid intelligence models – a new approach", *J. Steel Compos. Strucut*., **40**(3), 461-479. https://doi.org/10.12989/scs.2021.40.3.461.

Madas, P. and Elnashai, A.S. (1992), "A new passive confinement model for the analysis of concrete structures subjected to cyclic and transient dynamic loading", *J. Earthq. Eng. Struct. Dyn.*, **21**, 409-431. https://doi.org/10.1002/eqe.4290210503.

Mander, J.B., Priestley, M.J.N. and Park, R. (1988a), "Theoretical stress-strain model for confined concrete", *J. Struct. Eng*., **114**(8), 1804-1826. https://doi.org/10.1061/(ASCE)0733-9445(1988)114:8(1804).

Mander, J.B., Priestley, M.J.N. and Park, R. (1988b), "Observed stress-strain behavior of confined concrete", *J. Struct. Eng*., **114**(8), 1827-1849. https://doi.org/10.1061/(ASCE)0733-9445(1988)114:8(1827).

O'Shea, M.D. and Bridge, R.Q. (2000), "Desinge of circular thin-walled concrete filled steel tubes", *J. Struct. Eng*., **126**(11), 1295-1303. https://doi.org/10.1061/(ASCE)0733-9445(2000)126:11(1295).

Popovics, S. (1973), "A numerical approach to the complete stress-strain curve of concrete", *Cement Concrete Res*., **3**(5), 583-599. https://doi.org/10.1016/0008-8846(73)90096-3.

Razvi, S. and Saatcioglu, M. (1999), "Confinement model for high-strength concrete", *J. Struct. Eng*., **125**(3), 281-288. https://doi.org/10.1061/(ASCE)0733-9445(1999)125:3(281).

Richart, F.E., Brandtzaeg, A. and Brown, R.L. (1928), "A study of the failure of concrete under combined compressive stresses", *Report No. 12, Engineering Experiment Station, College of Engineering*, University of Illinois at Urbana Champaign, Champaign, IL, USA.

Saatcioglu, M. and Razvi, S.R. (1992), "Strength and ductility of confined concrete", *J. Struct. Eng*., **118**(6), 1560-1607. https://doi.org/10.1061/(ASCE)0733-9445(1992)118:6(1590).

Sadd, M.H. (2004), *Theory, Applications, and Numerics,* Cambridge, Massachusetts: Academic Press.

Saisho, M., Abe, T. and Nakaya, K. (1999), "Ultimate bending strength of high-strength concrete filled steel tube column", *J. Struct. Constr. Eng*., AIJ. **64**(523), 133-140.

Sakino, K. and Hayashi, H. (2004a), *Behavior of Concrete Filled Steel Tubular Stub Columns Under Concentric Loading*, Proceedings of the Third International Conference on Steel-Concrete Composite Structures, Wakabayashi, Japan, March.

Sakino, K., Nakahara, H., Morino, S. and Nishiyama, I. (2004b), "Behavior of Centrally Loaded Concrete-Filled Steel-Tube Short Columns", *J. Struct. Eng*., **130**(2) 180-188. https://doi.org/10.1061/(ASCE)0733-9445(2004)130:2(180).

Schneider, S.P. (1998), "Axially loaded concrete-filled steel tubes", *J. Struct. Eng*., **124**(10), 1125-1138. https://doi.org/10.1061/(ASCE)0733-9445(1998)124:10(1125).

Sun, Y. (2008), *Proposal and Application of Stress-Strain Model for Concrete Confined by Steel Tubes*, the 14th World Conference on Earthquake Engineering, Beijing, China, October.

Tang, J., Hino, S., Kuroda, I. and Ohta, T. (1997), "Analytical Study on Elasto-Plastic Flexural Behavior of Concrete-Filled Circular Steel Tubular Columns", *J. Memoirs of the Kyushu University. Faculty of Eng*., **57**(1), 37-52.

Tomii, M., Yoshimura, K. and Morishita, Y. (1977), *Experimental Studies on Concrete Filled Steel Tubular Stub Columns under Concentric Loading*, Proceeding of the International Colloquium on Stability of Structures Under Static & Dynamic Loads, New York, USA.

Wang, Q., Shi, Q., Xu, Z. and He, H. (2019), "Axial capacity of reactive powder concrete filled steel tube columns with two load conditions", *J. Steel Compos. Struct*., **31**(1), 13-25.

Wei, J., Luo, X., Lai, Z. and Varma, A.H. (2020), "Experimental behavior and design of high-strength circular concrete-filled steel tube short column", *J. Struct. Eng*., **146**(1). https://doi.org/10.1061/(ASCE)ST.1943-541X.0002474.

Yamamoto, T., Kawaguchi, and J. Morino, S. (2002), "Experimental study of the magnitude effect on the behaviour of concrete filled circular steel tube columns under axial compression", *J. Struct. Constr. Eng*., 237-244.

Yu, M., Zha, X., Ye, J. and She, C. (2010), "A unified equation for hollow and solid concrete-filled steel tube columns under axial compression", *J. Eng. Strucut*., **32**(4), 1046-1053.

CC